OE Optical Engineering

RESEARCH PAPER

Broadband 920-nm mirror thin film damage competition

Raluca A. Negres,[a,*] Kyle R. P. Kafka,[b] Chris Smith,[b] Marek Stehlik,[b] Sarah Olandt,[b] Amy Rigatti,[b] and Stavros G. Demos[b]

[a]Lawrence Livermore National Laboratory, Livermore, California, United States
[b]University of Rochester, Laboratory for Laser Energetics, Rochester, New York, United States

ABSTRACT. The 2023 Laser Damage conference thin-film damage competition was devoted to a survey on the state-of-the-art broadband near-IR multilayer dielectric (MLD) mirrors designed for ultra-short pulsed laser applications. The requirements for the coatings were a minimum reflection of 99.5% at 45-deg incidence angle for S-polarization from 830 nm to 1010 nm and group delay dispersion (GDD) < ± 50 fs^2. The participants were allowed to select the coating materials, coating design, and coating deposition method. Samples were damage tested at a single testing facility to enable direct comparison among the participants using a 25 ± 5 fs optical parametric chirped-pulse amplification (OPCPA) laser system operating at 5 Hz. The testing results from this set of 37 samples showed that dense coatings by ion-beam sputtering (IBS), magnetron sputtering (MS), and electron-beam ion assisted deposition (e-beam IAD) exhibited highest damage initiation onset (laser-induced damage threshold or LIDT) while e-beam coatings were low performers. In addition, multilayer coatings using tantala and/or hafnia as high index materials were top performers. Furthermore, this competition included for the first time the measurement of the damage growth onset (laser-induced damage growth threshold or LDGT). This latter performance metric plays an important role in establishing the safe operational conditions for larger aperture ultrashort pulsed lasers. Information pertaining to the morphology of the damage sites and their evolution under subsequent exposure to different laser fluences leading to damage growth is presented. Finally, not all coating samples in the survey met the GDD requirements stated above and associated measurements are discussed in the context of the present and past thin-film damage competitions focused on similar broadband near-IR MLD coatings.

Keywords: multilayer dielectric coatings; laser damage initiation; laser damage growth; femtosecond pulses; near-IR; broadband high reflectors; group delay dispersion

Paper 20240547SS received May 28, 2024; revised Aug. 7, 2024; accepted Aug. 8, 2024; published Oct. 4, 2024.

1 Introduction

The aim of the 2023 laser damage conference thin-film damage competition (representing the 16′th in a series of damage competitions started in 2008[1] at the Boulder Damage Symposium and now the SPIE Laser Damage Symposium) was to survey the laser damage resistance of state-of-the-art high reflector (HR) coatings in the near-IR spectral range designed for ultra-short pulsed lasers demanding high reflectivity and low group delay dispersion (GDD) over a broad spectral range.

*Address all correspondence to Raluca A. Negres, negres2@llnl.gov

The recent Basic Research Needs (BRN) Workshop in laser technology held in Washington, DC, United States outlined the need for ultra-short high-intensity/power laser sources to enable basic science applications.[2] In that context, advances in high field science applications, such as quantum electrodynamics, lab-astrophysics, electron and light sources, laser wakefield acceleration, etc., require high peak and/or high average power lasers with intensities reaching 10^{24} W/cm^2 or 100 TW power using ∼30-fs pulses at kHz repetition rates.[3] Moreover, PW-class lasers (modest repetition rates, ∼20 to 100 fs pulse durations) in operation and upcoming around the world do rely on high damage resistance optical coatings for beam transport and pulse compression. Meeting simultaneously laser-induced damage thresholds (LIDT) per the laser design along with several other stringent specifications of optical components (e.g., wavefront, reflectivity, and GDD) is challenging.[4,5] The organization of this thin film competition was motivated by the need to explore the current state-of-the-art in MLD coatings and also introduce the importance of meeting both high LIDT and laser-induced damage growth threshold (LDGT) specifications. Although some of the prior competitions distinguished "catastrophic" (growing) damage from "stable" (non-growing or functional) damage,[1] the present work represents the first inclusion of a systematic damage growth threshold characterization.

The spectral and temporal profiles of the laser used for damage testing should be ideally identical to those of the intended laser system that the optic will be used for. However, for the case of ultrashort pulsed lasers (typically shorter than about 20 fs) that necessitate use of transport mirrors with response over wide spectral bandwidths (on the order of 200 nm for near-IR pulses), nontrivial spectral shapes may be encountered, especially for systems employing nonlinear optical processes, such as optical parametric chirped pulse amplification (OPCPA). Therefore, it may not be practically possible to exactly reproduce the application's laser system temporal and spectral shape within the damage test systems available at different facilities. To mitigate this issue, the approach adopted in this work is twofold. First, experiments are performed at a single testing facility to enable direct comparison among the participating samples. Second, all samples will be damage tested at three different wavelengths within the designed bandwidth using pulses with slightly longer temporal durations and narrower spectral content. This approach will provide the overall damage resistance of the coatings for the general case and inform the performance as a function of the specific spectral shape of the operational pulse. Details of the deposition processes, cleaning method, coating materials, and layer count are shared.

The resulting damage thresholds as a function of wavelength are expected to be related to the internal electric-field intensity (EFI) for those respective wavelengths, which is strongly dependent on the coating design (as well as other fabrication parameters). Moreover, the narrower-spectrum results (due to longer pulse duration, thus lower peak intensity) may overestimate the fluence for damage onset only slightly while providing the wavelength-dependent comparison between samples correctly. The combined results as a function of wavelength will be representative of expected coating behaviors at shorter pulses and can be correlated with the corresponding spectral shapes.

2 Materials

2.1 Participation

A total of 37 samples were submitted for the 2023 competition by 19 different companies/institutions (majority with multiple entries) representing 8 different countries as detailed in Table 1. The samples were manufactured by each participant on their own 50-mm diameter by ∼3 to 10 mm thick substrates, which were then submitted for laser damage testing. In addition to providing the coating samples, participants were required to supply the following information:

- number of coating layers,
- coating materials,
- reflectance scans over the specified spectral bandwidth,
- a brief description of the deposition method,
- a brief description of the cleaning method, and
- substrate material.

Table 1 List of contributing companies or institutes, countries of origin, and number of years participating in the Laser Damage Symposium thin film damage competition series to date.

Company/institute	Country	Years of participation
Alpine Research Optics	United States	7
Altechna	Lithuania	4
Leybold Bühler Alzenau GmbH	Germany	1
Edmund Optics	United States	4
Edmund Optics	Japan	1
Institute Fresnel	France	2
Laser Components	Germany	14
Laserhof Frielingen GmbH	Germany	10
LaserOptik GmbH	Germany	9
Layertec	Germany	8
Laser Zentrum Hannover, e.V.	Germany	16
Research Electro-Optics, Inc.	United States	5
RhySearch	Switzerland	5
Runkun Optical Technology Co., Ltd.	China	2
SLS Optics	Isle of Man	11
Tongji University	China	12
UltraFast Innovations GmbH	Germany	1
Universal Thin Film Lab Corp.	United States	1
Veeco	United States	2

Finally, we encouraged additional sample details be shared that would make the survey results even more meaningful to the community at large, such as the presence of an overcoat top layer, any post-deposition or substrate treatments and/or specific deposition, and design or material parameters varied between multi-sample submissions from the same participant.

2.2 Sample Handling

Samples were assigned a unique two-digit participant code. The first digit consisted of a letter ranging from A to T and was assigned to each participant and the second digit was a sample number, 1 to 3, depending on how many samples were supplied by each participant. The connection between the participant name and code was unknown to the damage testing service to maintain anonymity; the test laboratory only had access to the participant code for reporting purposes. Only the participant codes are used in this report.

The high-reflectivity coatings had to meet the following specifications:

- reflectance >99.5% from 830 nm to 1010 nm,
- GDD < ± 50 fs^2 (target),
- incidence angle at 45 deg, S-polarization,
- vacuum test conditions: pressure <10^{-5} Torr, temperature (23 ± 2°C), and relative humidity (40 ± 20%), and
- no wavefront, stress, or surface quality requirements.

Table 2 2023 sample distribution as a function of coating deposition process.

Deposition process	Number of samples
IBS	21
e-beam	6
e-beam IAD	5
MS	5

Table 3 2023 sample distribution as a function of high refractive index coating materials.

High refractive index materials	Number of samples
HfO_2	12
Ta_2O_5 and HfO_2	9
Ta_2O_5	7
ZrO_2	2
Ta_2O_5 and Al_2O_3	2
Nb_2O_5	1
Ag	1
ZrO_2 and HfO_2	1
Nb_2O_5 and HfO_2	1
TiO_2 and HfO_2	1

We should note that GDD measurements by participants were not required to be supplied for entry; however, a commercial instrument was used by the test facility to measure all coating submissions and those results are being used in ranking of participants per GDD requirements listed above. The sample specifications for this year's damage competition are similar to the parameters specified in the 2016 damage competition centered on broadband low dispersion mirrors for 775 nm 40-fs pulses.[6]

Four deposition processes and seven high-index layer materials were sampled in the 2023 competition overall and are listed in Tables 2 and 3, respectively. SiO_2 was the low refractive index material used in all coatings. Most substrates were solvent cleaned before deposition either via ultrasonics or manual drag wiping; two substrates were super polished with no further cleaning while one other used *in-situ* oxygen plasma etching as pre-cleaning prior to deposition. In addition, all coatings were deposited on fused silica substrates.

3 Methods

3.1 Damage Testing

Damage testing was performed at a dedicated facility at the Laboratory for Laser Energetics (LLE) at 45-deg angle of incidence and vacuum conditions using a recently developed fs-damage testing system, which is illustrated in Fig. 1(a) (adapted with permission from Ref. 7 with annotations). For the purpose of this study, we highlight a few important characteristics of the damage test capability in Fig. 1(a).

1. Laser source is a custom OPCPA system (model Ultraflux by EKSPLA) operating at 5-Hz repetition rate with tunable central wavelengths from 820 nm up to 970 nm. For this study,

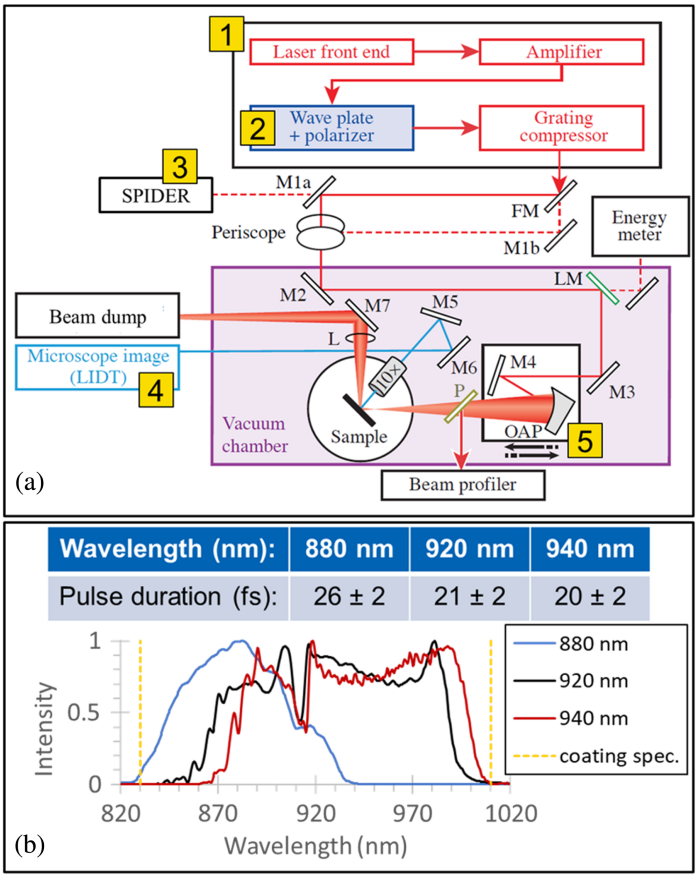

Fig. 1 (a) Schematic of performance characterization apparatus adapted from Ref. 7. FM, flip mirror, M#, mirror, LM, leaky mirror, OAP, off-axis parabolic mirror, P, pickoff, 10× = 10X microscope objective lens, and L, lens. Annotations 1–5 are discussed in the text. (b) Damage testing of HR samples in the survey was performed at each of three overlapping spectral bands centered at 880-, 920-, and 940-nm and covering the coatings' reflectivity band specifications above. The pulse durations of transform limited pulses associated with these spectral bands are also listed in the table.

three overlapping spectral bands were chosen within the reflectivity spectral band of the HR samples and are listed in Fig. 1(b), i.e., centered at 880-, 920-, and 940-nm and pulse durations of 26 ± 2 fs, 21 ± 2 fs, and 20 ± 2 fs, respectively.

2. Energy adjustment is performed prior to the compressor section using an achromatic wave-plate and Glan–Taylor polarizer to provide high-contrast attenuation while minimizing the impact on the spatial and temporal profiles due to B-integral.
3. Characterization of the temporal profile is performed with spectral phase interferometry for direct electric-field reconstruction (SPIDER by APE).
4. *In-situ* damage detection relies on dark field microscopy using 450-nm laser illumination.
5. Beam size on target can be adjusted by translation of the parabolic mirror to allow damage growth studies, i.e., using a beam format that is larger than the starting, as-initiated damage morphology.

Figure 2 illustrates (a) the test beam profile for irradiation at 920-nm and *in-situ* observations of damage initiation (i.e., any laser-induced modification of the coating) onset leading to (b) catastrophic and (c) non-catastrophic damage as well as (d) damage growth of a precursor (ablation crater), respectively. Specifically, for both damage initiation and growth studies, the beam was formatted to $1/e^2$-diameter of 350 μm for all three center wavelengths and a 100-on-1 test protocol (i.e., exposure of individual site locations by 100 laser shots at the same nominal fluence) was utilized to assess the damage performance at fixed fluences. In contrast to damage

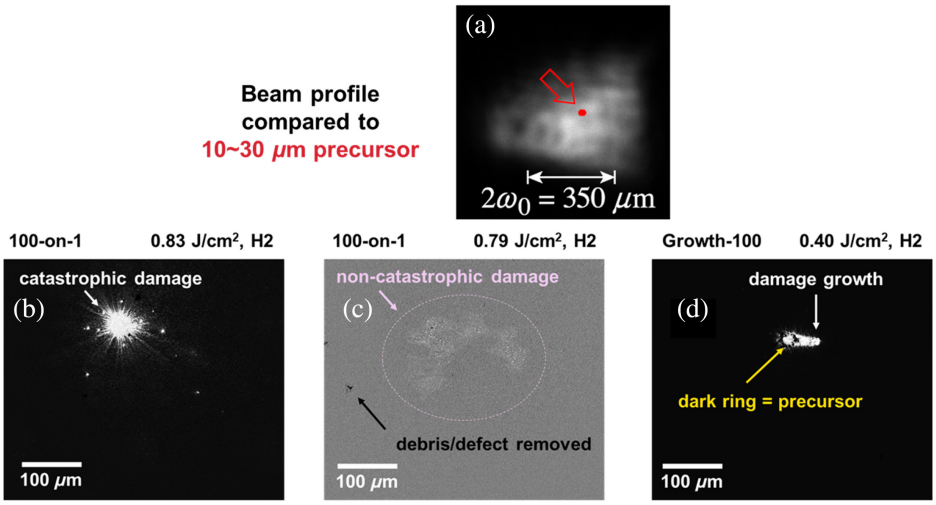

Fig. 2 (a) Test beam profile compared to damage growth precursor. (b)–(d) Example damage morphologies from background-subtracted, *in-situ* images for damage initiation (catastrophic and non-catastrophic), and damage growth, respectively. All examples shown are from sample H2 and laser exposures at 920 nm using the 100-on-1 test protocol at the fluence values noted above each image.

initiation performed at pristine coating locations, damage growth onset was performed at prior initiation sites where a "seed" damage site was first generated using 1-pulse and a ~60 μm beam diameter; the resulting ~10-30 μm diameter damage site served as a precursor for damage growth studies utilizing the larger format beam. Although the damage growth threshold experiment involved exposing the set of precursor sites to a range of laser fluences, each precursor was subjected to only 100 laser exposures at fixed fluence. Growth determination was done upon the observation of lateral increase in crater size after these exposures.

The reported LIDT values in this study typically correspond to non-catastrophic damage at pristine area locations. We note that debris/defect removal was sometimes observed [present as bright or dark specks in the *in-situ* images of Figs. 2(b) and 2(c)] and their number density varied among the samples; occasionally, such debris could seed the damage initiation and growth process. For consistency across all samples of this work, the LIDT and LDGT were determined using the *in-situ* microscopy system. Specifically, the LIDT and LDGT values reported here for each sample were computed as average values of highest- and lowest-fluences leading to "no damage" and "damage" for LIDT and "no growth" and "growth" for LDGT, respectively, along with error bars set by these lower and upper bounds (measurement uncertainties due to damage detection only); the absolute fluence values are subject to an additional estimated 5% instrumental error from beam profiling and energy measurement variations. It should be noted that the damage mechanisms in this short pulse regime are fairly deterministic so the fluence thresholds for damage initiation and growth are very abrupt and repeatable. More details on the damage test procedures, *in-situ* observations, damage probability calculations, and reporting of results can be found in Ref. 7.

3.1.1 *Damage morphology*

To gain better insight into the morphology of the damage initiation sites and to validate the in-situ observations, offline differential interference contrast (DIC) microscopy at test locations was performed in representative samples. However, for consistency across all samples in this work, the LIDT and LDGT values were determined using the *in-situ* detection only, mainly due to the time constraints in performing the damage testing for the large sample set in this survey.

Typical damage initiation site morphologies are illustrated in Fig. 3. At fluences below the onset of catastrophic damage, a rippled texture was often observed. In some samples, the ripples are bright and well defined as in Figs. 3(a) and 3(b), whereas in other samples the ripples are less distinct and are accompanied by a color-change modification, as in Figs. 3(c) and 3(d). However,

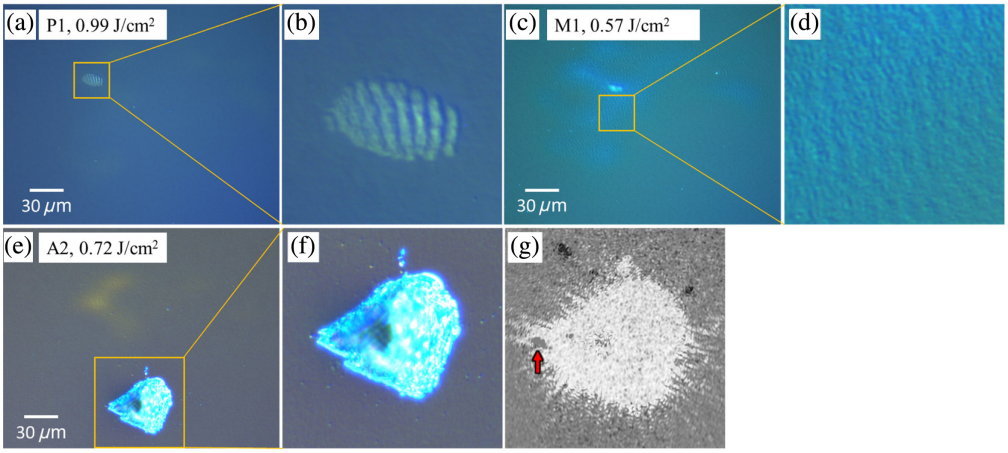

Fig. 3 Select offline microscopy images of typical damage initiation sites using 100-on-1 test protocol at the laser fluences noted in the labels of each image. (a, b) and (c, d) Non-catastrophic damage at pristine area locations from samples P1 and M1, respectively. (e, f) Color-change and catastrophic damage modes from sample A2. (g) Corresponding *in-situ* image after background subtraction from catastrophic damage site shown in panel (f). See text for more details.

the LIDT values quoted below, in almost all cases, are associated with the onset of the color-change mode revealed in DIC microscopy, as shown in Fig. 3(e) for yet another sample. In addition, as noted above in Sec. 3.1 for some of the samples, debris (particles or other defects) were present on the surface at the test locations, leading to catastrophic damage initiation and growth even in the lower-intensity portions of the irradiating beam. For example, the color change modification in Fig. 3(e) coincided with the peak-intensity location of the laser beam onto the sample, whereas catastrophic damage initiated off-center from a small precursor, likely a particle or a nodule, and grew catastrophically to a teardrop-shape over the course of the 100-pulse exposure [as shown in Fig. 3(f)]. Indeed, the corresponding *in-situ* image after background subtraction in Fig. 3(g) shows a dark spot at the leftward point of the damage site, indicating the initial precursor position at the tip of the arrow. The damage morphologies of these particle-mediated catastrophic sites are consistent with the morphologies observed in the damage growth testing protocol. This phenomenon was neglected, when possible, for the 100-on-1 LIDT determination, in favor of LIDT values from pristine locations. Finally, we note that the offline DIC microscopy was able to detect the onset of color-change modifications at about 10% lower fluences than detections based on the *in-situ* dark-field microscopy, though it is unclear if this initial phase modification affects the optical performance of the coatings.

DIC microscopy was also performed at damage growth sites, and representative images at different laser fluences are shown in Figs. 4(a)–4(e) from sample C1, as indicated within the labels for each thumbnail. We note that Fig. 4(a) is showing the initial "seed" damage site for growth testing. A number of salient damage growth behaviors can be appreciated based on these images.

1. Below the LDGT fluence (~0.39 J/cm^2 for sample C1), damage growth is not observed and the precursor damage site is nominally unchanged.
2. In general, the damage site growth boundaries are defined along lines that have either positive or negative angles with respect to the beam propagation direction along the plane, depending on the laser fluence. As a result, for higher fluences, the shape of the growing damage site can be approximated by a trapezoid while a triangular shape is observed at lower fluences.
3. The base of either the trapezoid or the triangle is anchored on the initial damage site and is not changing very much upon increasing the laser fluence. In contrast, following exposure to 100 pulses, the growing site has evolved preferentially along the laser beam propagation direction (to the right, orthogonal to the base).
4. Consequently, near the growth onset fluence [see Fig. 4(b)], the final grown site has a more triangular shape while higher fluences lead to a trapezoidal shape having a larger base away from the initial "seed."

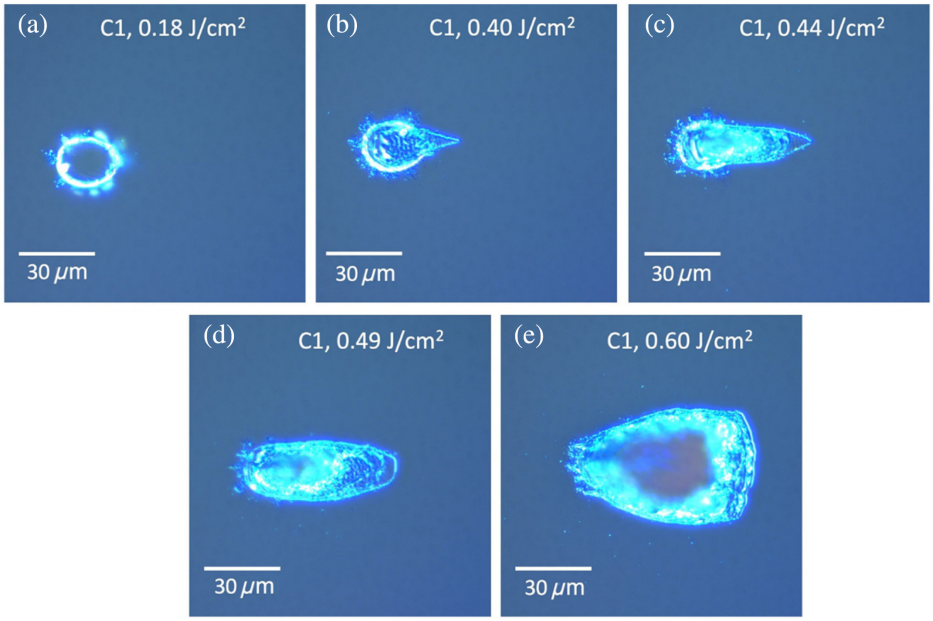

Fig. 4 (a)–(e) Typical final damage morphologies from sample C1 after 100 pulse-irradiation growth test at pre-initiated sites versus laser fluence. See text for more details.

5. At high fluences [see Fig. 4(e)], the damage site can grow in depth, eventually reaching the substrate.

The LDGT for all samples was determined by the onset of a feature similar to that illustrated in Fig. 4(b); however, due to relatively low scattering intensity generated by the damage growth feature in comparison to that from the precursor damage site, the *in-situ* imaging may be limited in the detection of subtle features smaller than about 5 μm, despite the 1 μm resolution of the *in-situ* microscope.

3.2 GDD Measurements

In addition to damage initiation and growth testing, GDD measurements were also performed on all coating samples in the survey using a Chromatis™ production-grade test instrument at LLE over the entire spectral range, at use conditions except the ambient humidity (56% relative humidity). The GDD spectral scans are presented in Figs. 5(a) and 5(b). Upon examining the data, we found that only 18 out of 37 samples strictly meet the original GDD requirements delineated by solid (green) horizontal lines (i.e., $< \pm 50$ fs^2) in the 830-1010 nm spectral range. We thus considered two alternative less strict specifications, either by relaxing the upper and lower bounds, i.e., GDD $< \pm 100$ fs^2 (the entire white plot area) or considering GDD $< \pm 50$ fs^2 over slightly narrower spectral range (the shaded green region) in Fig. 5(a). By using the latter relaxed-specification, the sample population was divided into groups using a "pass" or "fail" criteria, as shown in Figs. 5(a) and 5(b) having 27 and 10 samples, respectively. It should be noted that laser designers and optical manufacturers are presented with several grand challenges to meet all the desired coating specifications for current state-of-the-art broadband high reflectors for ultrashort pulsed lasers, including high reflectivity, damage resistance, and low GDD, and thus trade-offs similar to what we consider here are common practice.

4 Results and Discussion

The damage testing results of the 2023 survey comprised of 37 samples are summarized in the chart of Fig. 6, which illustrate the measured LIDT values versus wavelength (blue, gray, and orange bars correspond to central wavelengths and pulse durations indicated in Fig. 1(b), respectively) and LDGT values at 920 nm (hashed bars) as a function of sample code. Each bar represents the mean fluence value derived from the highest- and lowest-fluence with "no damage" and "damage," initiation or growth, respectively, and the error bars reflect the measurement

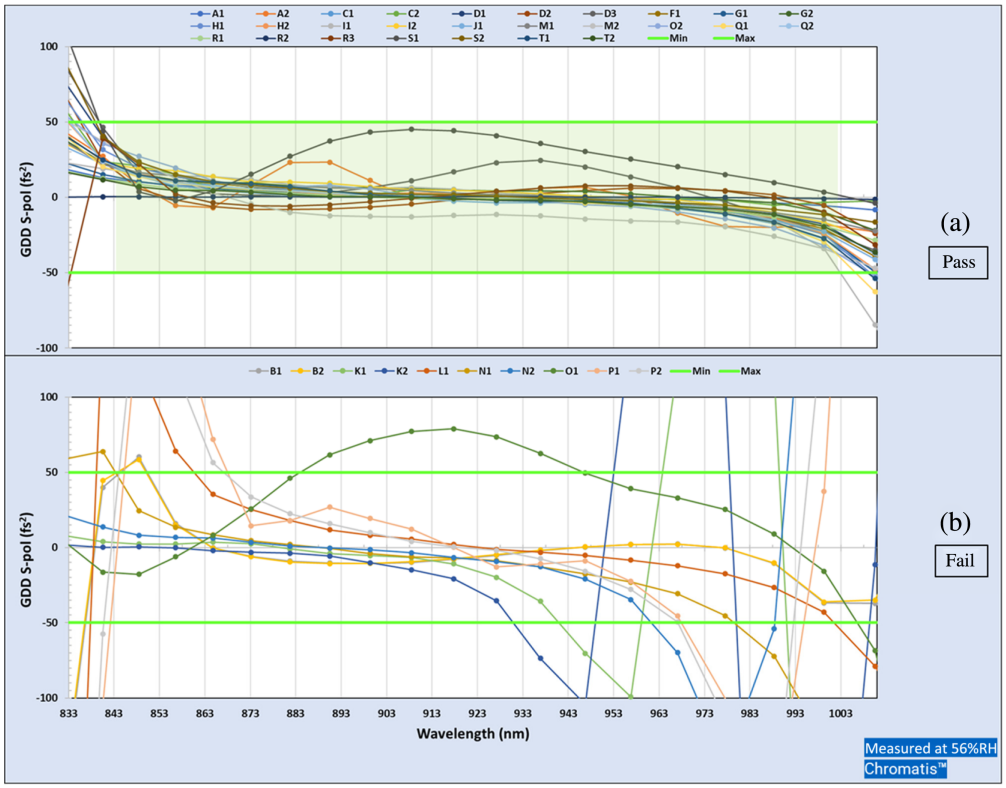

Fig. 5 GDD measurements performed on all 37 samples (labeled by two-digit codes) over the ~830-1010 nm spectral range at 45 deg incidence angle and S-polarization. (a) 27 coating samples that "pass" and (b) 10 coating samples that "fail" the relaxed GDD specifications (see discussion in the text), respectively. The original GDD requirements are bounded by the solid (green) lines at ± 50 fs^2 across the entire spectral range, whereas the entire plot area (white) or the shaded green box represent some practical trade-offs in GDD specifications.

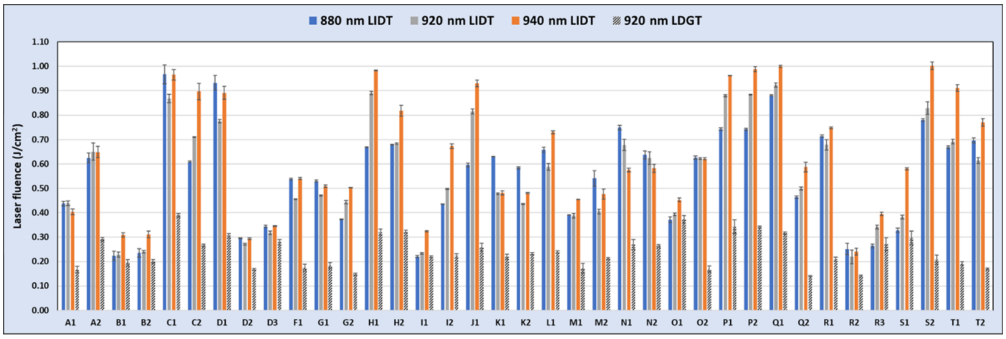

Fig. 6 Damage resistance upon fs-pulse irradiation of broadband HR coatings at 45 deg, S-polarization versus participant code. For each one of the samples in the population, four measurements are plotted, namely LIDT at three different central wavelengths (880-, 920-, and 940-nm) and LDGT at 920 nm, respectively. Mean fluence values and associated error bars (measurement uncertainties) were derived from the highest- and lowest-fluence with "no damage" and "damage" initiation and growth, respectively.

uncertainties due to damage detection. The results indicate that the LIDT dependence on wavelength varies across the sample population, with most trending up or down monotonically with wavelength while a few others exhibit a peak or a valley in LIDT value at the central wavelength of 920 nm.

To simplify the charts and examine the trends across the entire population, Fig. 7(a) shows only the lowest LIDT (out of the three measured wavelengths) along with the corresponding

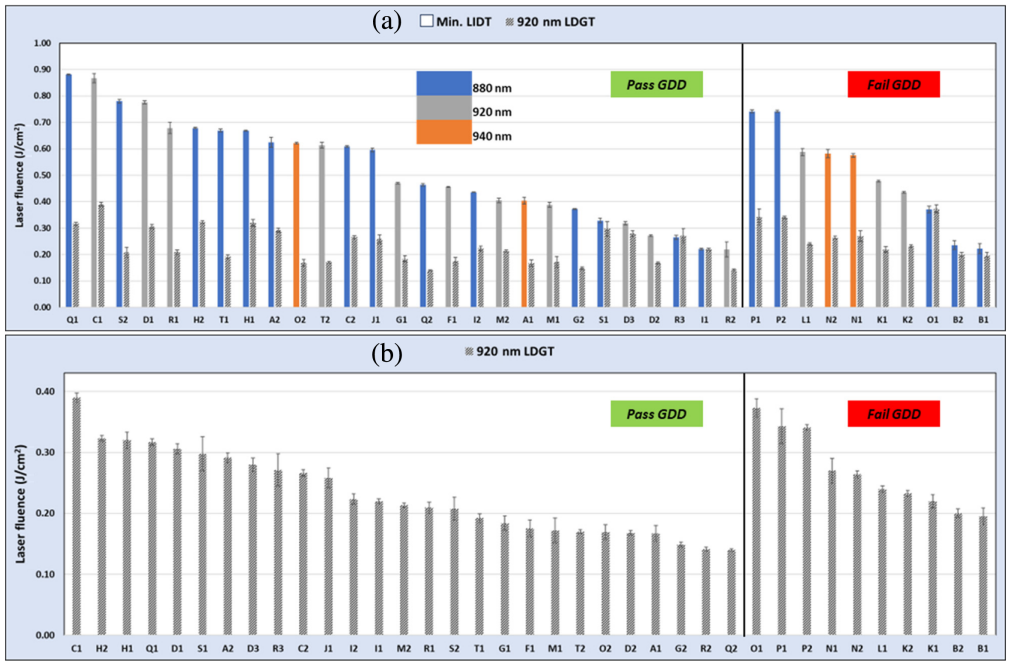

Fig. 7 Summary results of 2023 survey of 37 samples: (a) minimum LIDT and (b) LDGT, respectively, observed upon fs-pulse irradiation of broadband HR coatings at 45 deg, S-polarization. Samples denoted by participant codes were grouped based on the GDD measurements in Figs. 5(a) and 5(b), i.e., "pass" and "fail" GDD specifications.

LDGT values for each sample. Furthermore, samples will be grouped by "pass" or "fail" with respect to the GDD specifications (27 and 10 samples, respectively). The minimum LIDT or LDGT values are then sorted from high to low in each grouping and plotted in Figs. 7(a) and 7(b). The top chart includes both LIDT and LDGT results side by side to better illustrate a few salient behaviors.

1. Sample rankings across the sample population depend on which metric is used, either LIDT or LDGT, as shown in Fig. 7(a) versus Fig. 7(b), respectively; in other words, there is only a moderate correlation between LIDT and LDGT values such that the best performing coatings by LIDT are not necessarily the best performers by LDGT and vice-versa. The LDGT values are generally significantly reduced compared to LIDT ($\leq 50\%$ of LIDT) for most samples, and only the lowest performing samples in each group exhibit similar damage initiation and growth onsets [such as samples R3, I1, O1, or B1 in Fig. 7(a)].
2. The results indicate a $\sim 4:1$ range in minimum LIDT values across the sample population (vary from 0.88 to 0.22 J/cm^2) while the range in LDGT values is $\sim 3:1$ (vary from 0.39 to 0.14 J/cm^2).
3. There is an apparent correlation between GDD spectral shape and LIDT (illustrated in Fig. 8); the best performing samples exhibit mostly flat slowly varying GDD versus wavelength (which is characteristic of quarter-wave stack designs), in contrast to the spectral shapes from lower performing samples (which may be associated with engineered GDD designs). These trends are quite similar to those reported in 2016 competition,[6] which stated: (i) GDD is a direct consequence of coating design and (ii) intrinsic damage with fs-pulses is driven by the E-field inside the MLD stack, also a result of coating design; therefore, the correlation between GDD and LIDT is not surprising. However, a causality relationship between the GDD spectral shape and the wavelength-dependence of LIDT cannot be established with the information on hand and it is beyond the scope of this survey (further knowledge of MLD stack designs and expected E-fields within the individual coating layers may be needed).

The first observation above warrants more comments. The significant reduction of LDGT with respect to LIDT implies that the 1-pulse damage initiation ("seed") site introduces a

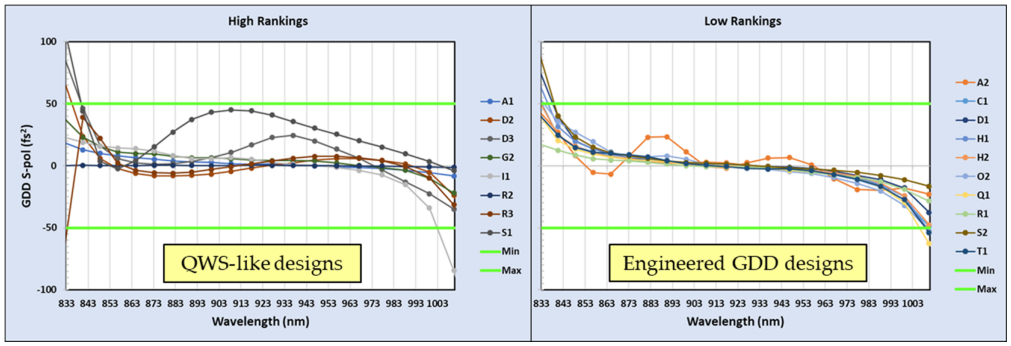

Fig. 8 GDD spectral shapes for selected high- and low-ranking coating samples from Fig. 7(a), which pass the relaxed GDD requirements.

significant EFI in comparison to the pristine coating. While in this case the ablation crater provided the initial EFI increase, an equivalent process presumably occurs for defect initiations, such as in Fig. 3(f), where a small damage crater is initiated by the particle or nodule on the first pulse and then catastrophically grows on subsequent pulses due to the EFI at that location. Although a simplified approach may have been to consider these irradiated defect locations as a damage initiation, the above reasoning suggests that this failure mode is more closely associated with damage growth. Therefore, the LIDT values were considered only for pristine (defect-free) locations, when possible, whereas any catastrophic failures due to occasional defects or contamination particles are neglected, with the assumption that LDGT carries that performance information. As such, the LDGT test may be an effective test to estimate coating performance robustness in the presence of defects, such as nodules or particle contamination.

The coating parameters are provided in Figs. 9(a) and 9(b) [in separate charts for sample sets that "pass" or "fail" GDD specifications, respectively, as in Figs. 7(a) and 7(b)]. The high-index materials are shown on the horizontal axis while samples are grouped according to their deposition method. For the former group of samples in Fig. 9(a), we conclude that the best performers used tantala and/or hafnia by ion-beam sputtering (IBS), magnetron sputtering

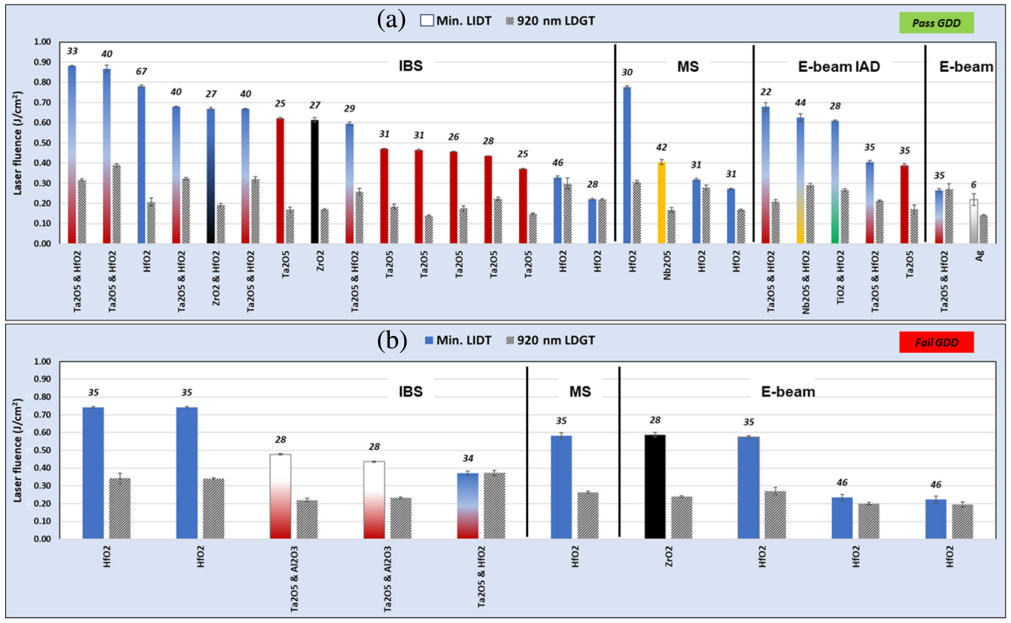

Fig. 9 Minimum LIDT and LDGT observed upon fs-pulse irradiation of broadband HR coatings at 45 deg, S-polarization versus high-index material used and coating deposition method for samples that (a) "pass" and (b) "fail" GDD specifications, respectively. The data are sorted high-to-low by minimum LIDT values within each grouping. The number of coating layers supplied by the participant is also shown above the LIDT column.

(MS), and electron-beam ion assisted deposition (e-beam IAD) while coatings by e-beam were low performers; even for the best LIDT coatings, damage growth can severely limit the safe operational conditions of high-repetition ultrashort pulsed lasers. By comparison, the samples in Fig. 9(b) that failed to meet GDD specifications had similar damage resistance (apart from the top performers Q1 and C1), used similar high-index materials, and exhibited comparable LDGT/LIDT ratios, i.e., ~0.4 to 1. In other words, GDD pass/fail grouping did not have a strong effect on the damage performance of the coatings, noting that the mean and standard deviation of minimum LIDT and LDGT values within the two subsets of samples were quite similar, i.e., $(0.52 \pm 0.20$ and $0.23 \pm 0.07)$ for the group in Fig. 9(a) versus $(0.50 \pm 0.18$ and $0.27 \pm 0.06)$ for the group in Fig. 9(b), respectively.

It is also instructive to look at multiple sample submissions by the same participant where a certain parameter is to be examined, i.e., post-deposition treatment, substrate cleaning, different coating designs using the same materials and deposition methods, etc. These sample pairs are denoted by the same letter and are separated by vertical lines in Figs. 10(a) and 10(b), with top labels providing the corresponding coating information within each group. Participants have explored consistency in performance from sister samples (deposited in the same coating run, such as B1-B2, P1-P2, and K1-K2) following different substrate cleaning or thermal annealing. Others have submitted different coating designs deposited by MS using different machine parameters (D1-D3). In addition, samples G1-G2 and H1-H2 have used different coating designs and high index materials by IBS. Finally, Fig. 11 illustrates additional parameters of interest to the participants, such as the effects of adding hafnia layers at the top of the MLD stack for superior

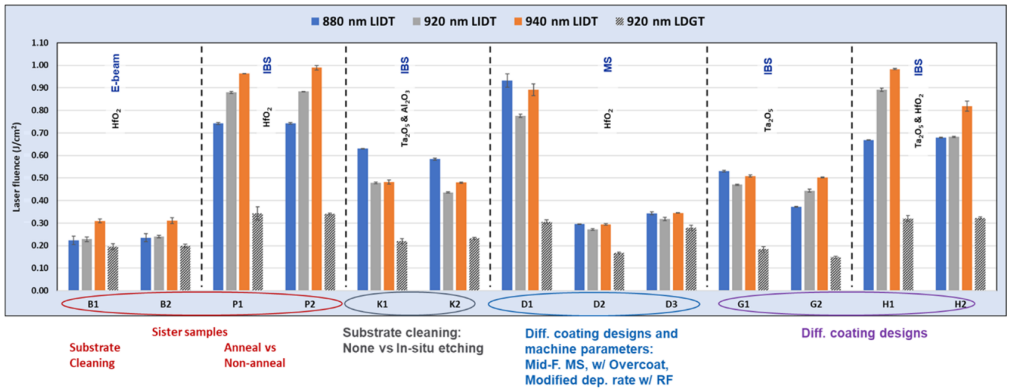

Fig. 10 The relative comparison in performance of coating pairs, each using the same high-index materials and deposition methods with varying substrate cleaning, post-deposition treatment, machine parameters, or coating designs.

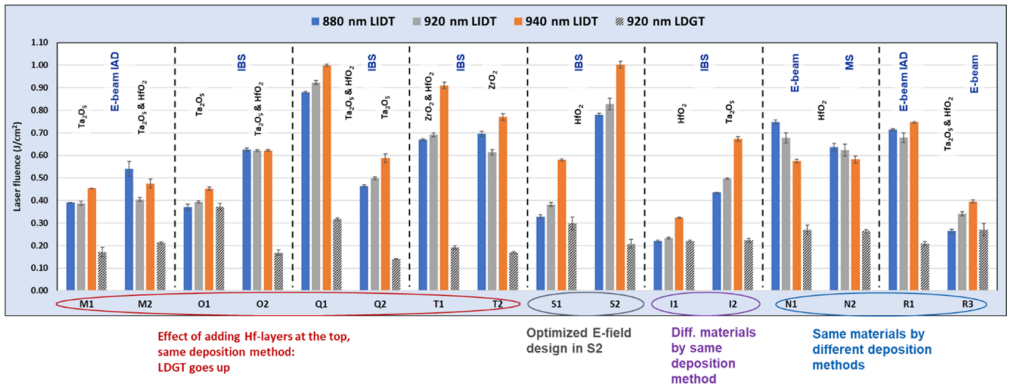

Fig. 11 The relative comparison in performance of coating pairs with additional top hafnia layers, optimized E-field design, and different high-index materials by the same deposition method and vice-versa.

LDGT, E-field optimization, using different high-index materials by the same deposition method and vice-versa.

5 Summary

This study explored the damage behavior of state-of-the-art broadband near-IR multilayer dielectric mirrors designed for ultra-short pulsed laser applications. The testing protocols introduced two novel elements designed to provide a more complete characterization of the damage performance of the coatings, namely measurements of both damage initiation at three different wavelengths within the spectral band of interest and damage growth thresholds.

We found that multilayer coatings using tantala and/or hafnia as high index materials were top performers within several coating deposition groups. Specifically, dense coatings by IBS, MS, and e-beam IAD exhibited the highest damage initiation onset (laser-induced damage threshold, or LIDT), and e-beam coatings were low performers. In addition, damage growth onset (laser-induced damage growth threshold or LDGT) was also examined. The GDD measurements revealed that ~73% of the samples received (27 out of 37 total) met the relaxed GDD specifications ($< \pm 100$ fs^2) over the 830-1010 nm spectral bandwidth and only 18 samples strictly passed the original GDD requirements of $< \pm 50$ fs^2.

In conclusion, the best performing samples in the 2023 survey of broadband 920-nm fs-laser mirrors were C1 and Q1, both coatings using Ta_2O_5 and HfO_2 and SiO_2 by IBS. For reference, Table 4 lists all the measured LIDT and LDGT values from these coating samples.

In the larger context of the annual thin film damage competitions to date and the observed global trends, Fig. 12 provides an updated summary[8] of the impact of wavelength, pulse length,

Table 4 Summary of LIDT and LDGT measured values (in J/cm^2) and associated measurement uncertainties due to damage detection for the top performing samples in the 2023 thin film damage competition.

Sample code	880-nm LIDT	920-nm LIDT	940-nm LIDT	920-nm LDGT
C1	0.97 ± 0.04	0.87 ± 0.02	0.97 ± 0.02	0.39 ± 0.01
Q1	0.88 ± 0.002	0.92 ± 0.01	1.00 ± 0.004	0.32 ± 0.01

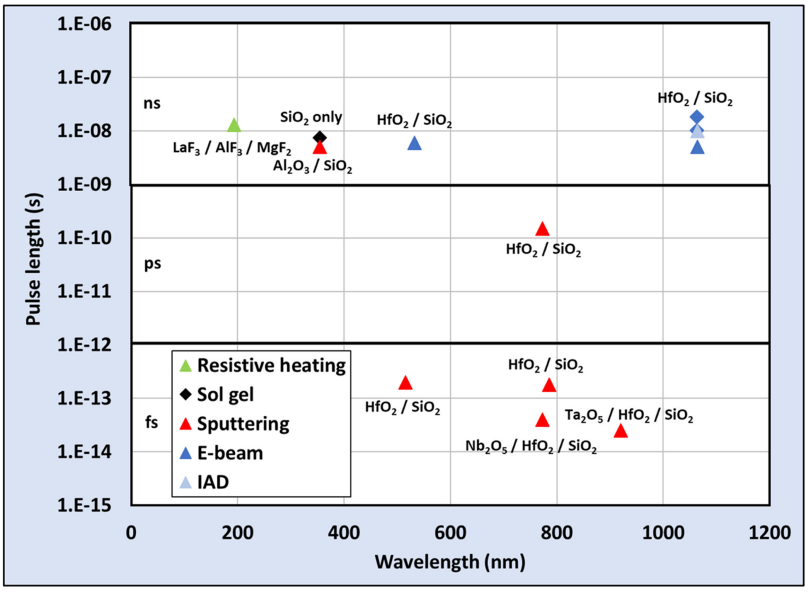

Fig. 12 Winning entries (coating materials and deposition processes) of thin film damage competitions to date as a function of wavelength and pulse length. (Adapted with permission from Ref. 8)

deposition process, and coating material on the highest damage threshold entries of each competition since 2008.

Code and Data Availability

The data that support the findings of this article are not publicly available to maintain the anonymity of the samples with respect to the participants in the survey in agreement to the rules of the thin film damage competition. They can be requested from the author at negres2@llnl.gov.

Acknowledgments

The authors acknowledge all of the 2023 participants who prepared samples and provided the relevant coating information; we recognize the significant investment to manufacture samples by these companies and research institutes. This paper is based in part on the SPIE Laser Damage conference proceedings.[9] This work was performed under the auspices of the U.S. Department of Energy (DOE) by Lawrence Livermore National Laboratory under Contract DE-AC52-07NA27344 (LLNL-JRNL-864653) as well as the Department of Energy [National Nuclear Security Administration] University of Rochester "National Inertial Confinement Fusion Program" under Award Number DE-NA0004144. This report was prepared as an account of work sponsored by an agency of the US Government. Neither the US Government nor any agency thereof, nor any of their employees, makes any warranty, express or implied, or assumes any legal liability or responsibility for the accuracy, completeness, or usefulness of any information, apparatus, product, or process disclosed, or represents that its use would not infringe privately owned rights. Reference herein to any specific commercial product, process, or service by trade name, trademark, manufacturer, or otherwise does not necessarily constitute or imply its endorsement, recommendation, or favoring by the US Government or any agency thereof. The views and opinions of authors expressed herein do not necessarily state or reflect those of the US Government or any agency thereof.

References

1. C. J. Stolz, M. D. Thomas, and A. J. Griffin, "BDS thin film damage competition," *Proc. SPIE* **7132**, 71320C (2008).
2. U.S. Department of Energy, "Report of basic research needs workshop on laser technology," Washington, DC (15–17 August 2023). https://science.osti.gov/-/media/ardap/pdf/2024/Laser-Technology-Workshop-Report_20240105_final.pdf
3. F. Albert et al., "2020 roadmap on plasma accelerators," *New J. Phys.* **23**(3), 031101 (2021).
4. LBNL, "Report of workshop on laser technology for k-BELLA and beyond," Berkeley, CA (9–11 May 2017). https://www2.lbl.gov/LBL-Programs/atap/Report_Workshop_k-BELLA_laser_tech_final.pdf
5. J. Zhu et al., "Introduction to SG-II 5 PW laser facility," in *OSA Tech. Digest*, p. SM1M.7 (2016).
6. R. A. Negres et al., "40-fs broadband low dispersion mirror thin film damage competition," *Proc. SPIE* **10014**, 100140E (2016).
7. K. R. P. Kafka, T. Z. Kosc, and S. G. Demos, "Methods and apparatus for comprehensive characterization of performance attributes and damage thresholds of ultrafast laser optics," *Opt. Eng.* **61**(7), 071605 (2022).
8. C. J. Stolz and R. A. Negres, "Ten-year summary of the Boulder Damage Symposium annual thin film laser damage competition," *Opt. Eng.* **57**(12), 121910 (2018).
9. R. A. Negres et al., "Broadband, 920-nm mirror thin film damage competition," *Proc. SPIE* **12726**, 1272606 (2023).

Biographies of the authors are not available.